Journal of Materials Chemistry A

PAPER

View Article Online
View Journal | View Issue

Cite this: J. Mater. Chem. A, 2019, 7, 4549

Highly efficient CO_2 capture by mixed matrix membranes containing three-dimensional covalent organic framework fillers†

Youdong Cheng, Linzhi Zhai, Yunpan Ying, Yuxiang Wang, Guoliang Liu, Jinqiao Dong, Denise Z. L. Ng, Saif A. Khan and Dan Zhao *

Received 27th October 2018
Accepted 23rd January 2019

DOI: 10.1039/c8ta10333j

rsc.li/materials-a

Mixed matrix membranes (MMMs) have long been considered as promising membrane types for industrial energy-intensive gas separation processes. Current MMMs are still facing grand challenges of poor filler dispersion and poor polymer-filler interfacial compatibility. The present study demonstrates that these challenges can be addressed by fabricating MMMs containing three-dimensional (3D) covalent organic framework (COF) fillers with ultrasmall size-selective pores. Two different polymer matrixes, including glassy 6FDA-DAM and rubbery Pebax, are explored to validate the effectiveness of 3D COF fillers in improving the membrane separation performance. The pure organic nature of COFs facilitates their high affinity with pure organic polymer matrixes, leading to good interfacial compatibility in the resultant MMMs. These porous COF-300 fillers can increase the membrane fractional free volume that enhances the membrane gas permeability. Besides, the ultrasmall pores of COF-300 fillers and the rigidified polymer chains at the filler surface can enhance the size discriminative processes, resulting in increased membrane gas pair selectivity. Moreover, the separation performance of COF-300 can be further improved by functionalizing it with polyethylenimine (PEI), enabling the design of advanced membranes suitable for industrial applications.

Introduction

The adverse effects on the environment and human health induced by massive amounts of CO_2 emitted during anthropogenic activities have aroused great concerns over the past decades.[1] Large-scale CO_2 capture and storage (CCS) has long been sought as an effective approach to mitigate CO_2 emission and therefore stop the rapid increase in its atmospheric concentration.[2] The conventional amine-based absorption process has been used for industrial CO_2 capture for decades, while its high energy penalty associated with absorbent regeneration severely limits its future as large-scale CCS.[2] Meanwhile, its large capital investment and complicated operational process render it less attractive for off-shore CO_2/CH_4 separation and other small-scale processes.[3] In contrast, membrane-based gas separation techniques offer an economically attractive and technologically viable alternative for CCS because of their high energy efficiency, low capital cost, small carbon footprint, and facile and continuous operation mode.[4] Up till now, tremendous efforts have been devoted to the development of novel membrane materials, ranging from conventional nonporous polymers to advanced porous polymers,[5] inorganics,[6] supported liquids,[7] and more recently, two-dimensional laminar materials.[8] Despite the exciting achievements in high-performance membrane materials, polymers still dominate the current gas separation market mainly due to their easy processability, robust mechanical strength and low production cost. However, the deployment of pure polymeric membranes for industrial CCS is largely hindered by the trade-off relationship existing between the membrane permeability and selectivity, known as the Robeson upper bounds.[9]

Therefore, various methods have been proposed to further improve the separation performance of current polymeric membranes, including polymer blending,[10] thermal-induced cross-linking,[11] novel polymer design[12] and filler incorporation.[13–15] Among them, the incorporation of nonporous or porous fillers into a polymer matrix leads to the formation of mixed matrix membranes (MMMs), which have aroused great interest in developing high-performance membranes. Until now, a large number of porous or nonporous materials have been incorporated as fillers in MMMs, including zeolite,[16] metal oxide,[17] mesoporous silica,[18] graphene and graphene oxide,[19] metal–organic frameworks (MOFs),[20–22] and more recently, covalent organic frameworks (COFs).[23] Among them, COFs have gained great attention owing to their pure organic nature, well-defined pore size and geometry, rich chemical functionality, good thermal and chemical stability. Notably, the pure organic

Department of Chemical and Biomolecular Engineering, National University of Singapore, 4 Engineering Drive 4, Singapore 117585. E-mail: chezhao@nus.edu.sg

† Electronic supplementary information (ESI) available. See DOI: 10.1039/c8ta10333j

nature of COF fillers resembles that of the polymer matrix, which can largely improve the affinity between the dispersed filler phase and the continuous polymer matrix phase. This compatibility improvement is crucial for homogeneous filler dispersion and elimination of nonselective voids in final MMMs. Since the first example of two-dimensional (2D) COF nanosheet fillers in MMMs reported in 2016,[23] various types of COFs with different linkages and pore sizes have been explored for diversified applications. For instance, Gascon *et al.* incorporated an azine-linked COF (ACOF-1) into a commercially available polymer Matrimid® 5218 to fabricate composite membranes for CO_2/CH_4 separation.[24] Compared to the pure polymeric membrane, the ACOF-1-containing MMM shows a one-fold increase in CO_2 permeability owing to fast transport of gases through the filler pores, coupled with a slightly increased CO_2/CH_4 selectivity due to the CO_2-philic properties of these porous fillers. Rahul *et al.* dispersed two different chemically stable COFs with relatively large pore sizes (TpPa-1: 18 Å and TpBD: 24 Å) into the PBI-BuI matrix with a filler loading of up to 50 wt%.[25] A nearly seven-fold increase in gas permeability was observed in MMMs compared to bare polymeric membranes ascribing to the fast gas permeation through the pores of COF fillers.

Despite the exciting achievements in COF-based MMMs, previous studies mainly focus on 2D COFs with relatively large pore sizes (>8 Å) that often fail to achieve a substantial increase in gas separation selectivity based on molecular size differences. Contrary to conventional 2D COFs built from planar monomers, three-dimensional (3D) COFs constructed by 3D building blocks can have more complicated structures.[26] 3D COFs are commonly featured by their interpenetration nature, therefore greatly reducing their effective pore sizes. For example, one 3D COF, COF-300, was reported recently possessing a 7-fold interpenetration that decreases its pore size down to 4 Å.[27] This ultrasmall pore size is close to the kinetic diameters of gas molecules, such as CO_2 (3.3 Å), N_2 (3.68 Å) and CH_4 (3.8 Å). Therefore, size-selective permeation of gases through the 4 Å pores can be anticipated in COF-300-based MMMs. Moreover, the high Brunauer–Emmett–Teller (BET) surface area of COF-300 (*e.g.*, 1360 $m^2 g^{-1}$)[28] outperforms that of previous 2D COF fillers (*e.g.*, 415 $m^2 g^{-1}$ for NUS-2,[23] 535 $m^2 g^{-1}$ for TpPa-1 (ref. 29)), rendering it as a suitable filler in constructing gas permeation highways in MMMs. Despite the extensive exploration of 2D COFs in MMMs, as far as we know, there still is a lack of study on 3D COF-based MMMs owing to the stringent requirements for the synthesis of 3D COFs with high crystallinity and ultrasmall pores. Therefore, here we report the exploration of COF-300 as fillers in two different polymer matrixes, namely glassy 6FDA-DAM and rubbery Pebax, to construct MMMs for efficient CCS (Fig. 1a). 6FDA-DAM demonstrates impressive CO_2/CH_4 and CO_2/N_2 separation performance in terms of high permeability and decent gas pair selectivity. The bulky $-CF_3$ functional groups in its rigid backbones prevent the efficient packing of polymer chains, resulting in a large membrane fractional free volume. As for Pebax, it is a commercially available rubbery polymer containing hard polyamide segments and soft polyether segments, possessing a promising CO_2 capture performance especially in the presence of water.[18] Moreover, the soft polyether segments in Pebax can efficiently wrap the porous fillers, which is beneficial for the fabrication of defect-free MMMs even at high filler loadings.[30] COF-300 crystals were prepared in a solvothermal reaction with an aging process to allow the formation of the thermodynamically stable phase with 7-fold interpenetration. The as-prepared MMMs demonstrate enhanced gas permeability owing to the fast gas transport channels built by the highly porous COF-300 fillers. Meanwhile, the size-selective pores of COF-300 and the polymer rigidification at the polymer-filler interface synergistically contribute to the increased gas pair selectivity. Moreover, the rich chemical tunability of COF-300 fillers prompts us to further functionalize them with polyethylenimine (PEI) to obtain COF@PEI hybrid fillers so as to improve the CO_2-philicity and polymer affinity of fillers in the resultant MMMs, facilitating the design and preparation of high-performance membranes for large-scale CCS.

Experimental

Materials

All the reagents are commercially available and used without further purification. 6FDA-DAM (M_n = 270 kDa, PDI: 2.68) was purchased from Akron Polymer Systems (USA). Pebax® MH 1657 was purchase from Arkema Pte Ltd (China). Poly(ethyleneimine) (PEI, M_n = 60 000, 50 wt% in H_2O) was acquired from Sigma-Aldrich. Tetra-(4-anilyl)methane (TAM, 95.0%), 1,4-dioxane (99.0%), and terephthaldehyde (BDA, 98.0%) were acquired from TCI. Chloroform ($CHCl_3$, 99.8%), acetone (99.5%), tetrahydrofuran (THF, 99.9%), acetic acid (99.7%), ethanol (99.5%) and methanol (99.8%) were purchased from Fisher Scientific.

Synthesis of COF-300

The synthesis of COF-300 was performed based on the published procedure.[27] Briefly, a 10 mL Pyrex tube was charged with TAM (40.0 mg, 0.104 mmol), BDA (24.0 mg, 0.178 mmol), and 1,4-dioxane (2.0 mL). The mixture was shortly sonicated to form a homogeneous solution, followed by the addition of acetic acid (0.4 mL, 6 M). After three freeze–thaw cycles under vacuum, the tube was allowed to stand at room temperature for 3 days and then heated at 80 °C for 3 days. This represents the aging process that enables the formation of a thermodynamically favoured crystalline phase with a 7-fold interpenetration structure.[27] Next, the tube was heated at 120 °C for 3 days to improve the crystallinity of the COFs. After cooling to room temperature, the yellow powder was filtered from the mother solution, washed with 1,4-dioxane, acetone, THF and methanol, separately. Finally, the obtained solid was solvent exchanged with methanol at least 3 times and heated at 120 °C under vacuum for 12 h to afford the final COF-300 products (yield: 78%).

Synthesis of COF@PEI

PEI was functionalized onto the surface of COF-300 according to a procedure published previously.[18] In a typical preparation, PEI (400 μL) was dissolved in methanol (20 mL) under continuous

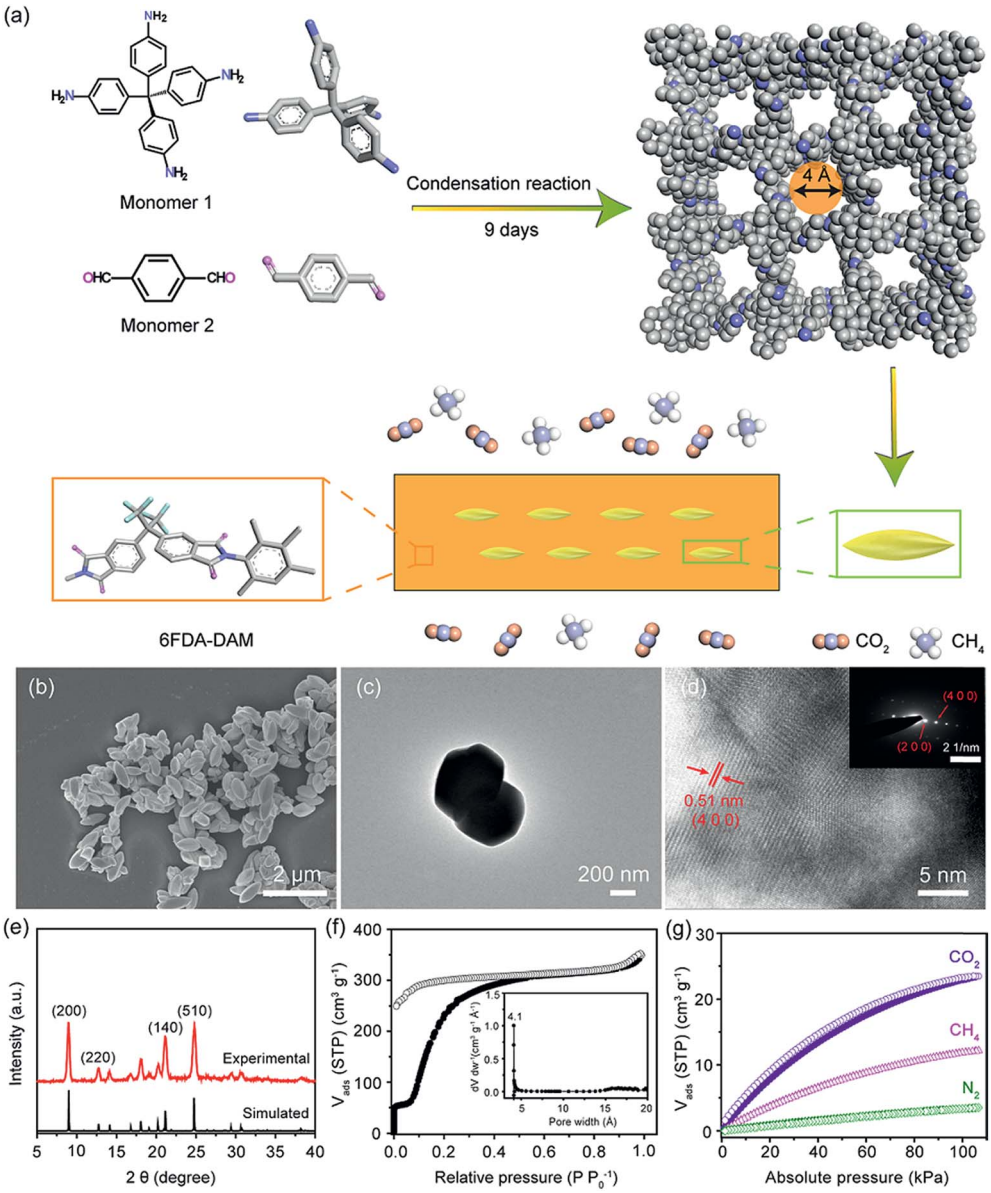

Fig. 1 (a) Schematic illustration of the preparation of COF-300 fillers and the fabrication of COF-300/6FDA-DAM MMMs for CO_2/CH_4 separation. (b) FESEM image of COF-300 crystals with a well-defined spindle shape. (c) TEM image of COF-300 crystals. (d) High resolution TEM image of COF-300 demonstrating an ordered lattice structure. The inset shows the SAED pattern of COF-300. (e) PXRD patterns of COF-300. The experimental pattern (top) matches well with the simulated pattern (bottom), indicating the successful preparation of high-quality COF-300 crystals. (f) N_2 sorption isotherm (77 K) of COF-300 crystals (adsorption: solid symbols; desorption: empty symbols). The inset shows the pore size distribution of COF-300 crystals calculated based on the slit mode using a Horvath–Kawazoe model. (g) CO_2, CH_4 and N_2 sorption isotherms of COF-300 collected at 298 K (adsorption: solid symbols; desorption: empty symbols).

stirring for about 2 min. The COF-300 powder (200 mg) dispersed in methanol (5 mL) was then gradually added to the PEI/methanol solution. The resultant mixture was refluxed at 90 °C for 2 h and then the products were recovered by centrifugation, washed with fresh methanol three times to remove the excess PEI. The obtained samples were dried at 120 °C under vacuum for 12 h and denoted as COF@PEI.

Preparation of membranes

All the membranes were prepared by the conventional solution-casting method. For 6FDA-DAM based MMMs, 6FDA-DAM was dissolved in $CHCl_3$ under continuous stirring for 4 h. A desired amount of COF-300 or COF@PEI powder was homogeneously dispersed in $CHCl_3$ (2 mL) under sonication. Next, the powder suspension was added dropwise into the polymer solution to get a 6 wt% membrane casting suspension. After being stirred at room temperature for 24 h, the resultant suspension was transferred onto a flat glass Petri dish. The membranes were slowly dried at room temperature for 2 days and heated at 100 °C under vacuum for 24 h. The pure 6FDA-DAM membrane was fabricated following a similar procedure without the addition of COF fillers.

As for Pebax-based MMMs, Pebax pellets were fully dissolved in an ethanol/water (70/30 wt%) mixture under reflux at 90 °C for 3 h. Then, a certain amount of COF-300 or COF@PEI powder was homogeneously dispersed in the Pebax solution under sonication to form a 6 wt% membrane casting suspension. The resultant suspension was stirred for 24 h and then poured onto a flat glass Petri dish, dried at room temperature for 3 days and further heated at 100 °C under vacuum for 24 h. The pure Pebax membrane was prepared following a similar procedure without the addition of COF fillers.

For simplicity, the as-prepared MMMs are denoted as filler/polymer-*x*, where the filler refers to either COF-300 or COF@PEI, the polymer refers to either 6FDA-DAM or Pebax, and *x* refers to the weight percentage of fillers in the final membranes (*e.g.*, COF-300/6FDA-DAM-7 stands for the MMM with the 6FDA-DAM matrix and 7 wt% of COF-300 fillers). The membrane thickness was about 60–100 μm, as measured using a digital micrometer.

Characterization

The crystallinity of COF-300, COF@PEI, and all membranes were tested by X-ray diffraction (XRD, Rigaku MiniFlex X-ray). The morphologies of COF-300, COF@PEI, and membranes were recorded using a field emission scanning electron microscope (FESEM, FEI Quanta 600). The shape and size of COF-300 and COF@PEI particles were recorded by transmission electron microscopy (TEM, JEOL-JEM 2010F). The thermal stability was evaluated by thermogravimetric analysis (TGA, Shimadzu DTG-60AH) in the temperature range of 70–800 °C under flowing air (25 mL min^{-1}). Fourier transform infrared spectroscopy (FTIR, Bio-Rad FTS-3500 ARX) was adopted to investigate the bond information in the materials. Differential scanning calorimetry (DSC, Perkin Elmer DSC 8000) analyses were performed to record the glass transition temperatures (T_g) of all the membranes at different testing temperature ranges (6FDA-DAM: 50–420 °C, Pebax: −60 to 300 °C) with a scanning rate of 10 °C min^{-1}. Gas sorption isotherms of CO_2, CH_4 and N_2 were measured up to 1 bar using a Micromeritics ASAP 2020 physisorption analyzer.

Gas permeation measurement

The permeability and selectivity of all membranes were determined by CO_2/CH_4 or CO_2/N_2 mixtures (50 : 50 vol%) at 25 °C in a Wicke–Kallenbach gas permeation setup.[21] The volumetric flow rates of the feed gas and sweep gas (argon) were maintained at 50 mL min^{-1} and 5 mL min^{-1}, respectively. The gas compositions at the permeate side were analysed using a gas chromatograph (Shimadzu GC-2014). All membranes were prepared at least three times to verify their reproducibility. The gas permeability (P_i, barrer, 1 barrer = 10^{-10} cm^3 (STP) cm cm^{-2} s^{-1} $cmHg^{-1}$) is defined by eqn (1),

$$P_i = \frac{Q_i l}{A \Delta P_i} \quad (1)$$

where Q_i is the volume flow rate of gases (cm^3 s^{-1}), l is the membrane thickness (μm), A is the effective area of the membrane (cm^2), and ΔP_i is the partial pressure difference across the membrane (cmHg). The mixed gas selectivity (α_{ij}) is calculated by eqn (2),

$$\alpha_{ij} = \frac{y_i / y_j}{x_i / x_j} \quad (2)$$

where x_i/x_j and y_i/y_j represent the molar fraction of i/j in the feed and permeate side, respectively. When the membranes were tested under moisture, both the feed and sweep gases were humidified by passing through water bottles at room temperature (relative humidity: ∼85%).

Results and discussion

Characterization of COF-300

COF-300 crystals were obtained in a spindle shape with an average particle size of ∼400 nm (width) × ∼1000 nm (length), as confirmed by FESEM and TEM images (Fig. 1b and c). Notably, the well-defined morphology of these COF-300 crystals differs significantly from that of the conventional 2D COFs synthesized using similar solvothermal reactions,[25] enabling the facile and homogeneous dispersion of COF-300 fillers in MMMs. The good crystallinity of as-synthesized COF-300 particles was evidenced by ordered lattice structures from the high resolution TEM image, with a periodic distance of 0.51 nm ascribing from the (4 0 0) plane (Fig. 1d). Besides, the selected area electron diffraction (SAED) pattern (inset in Fig. 1d) of COF-300 crystals displays the diffraction pattern of (h 0 0) planes, further demonstrating the long-range order within these covalently linked particles. The powder XRD (PXRD) pattern of the as-synthesized COF-300 corresponds well with the simulated pattern of COF-300 with a 7-fold interpenetration feature, providing strong evidence on the successful preparation of the desired products in a pure crystal phase. The FTIR spectra indicate the full consumption of the monomers owing to the disappearance of the –NH_2 stretching at 1609 cm^{-1} of TAM (monomer 1) and the C=O stretching at 1681 cm^{-1} of BDA (monomer 2, Fig. S1†). Moreover, the emergence of a strong peak at 1620 cm^{-1} ascribing to the stretching of C=N bonds in COF-300 unambiguously confirms the covalent linkage in the extended framework. It is well-known that imine-based COFs possess good chemical stability in common organic solvents and even water.[31] Therefore, COF-300 was soaked in water at room temperature for 3 days. The retention of crystallinity tested by PXRD validates the decent water stability of COF-300 (Fig. S2†), which is beneficial for maintaining the gas separation performance of COF-300-based MMMs under humid conditions. The permanent porosity of COF-300 was probed using the N_2 sorption isotherm collected at 77 K, indicating the highly porous nature of COF-300 with a BET surface area of 1209 m^2 g^{-1} (Fig. 1f). This is comparable to the reported value of 1360 m^2 g^{-1} in the literature.[28] The pore size distribution of as-synthesized COF-300 shows a major peak at 4.1 Å (inset in Fig. 1f), which corresponds well with the value calculated from the crystal model (4.0 Å). It is worth mentioning that these ultrasmall pores in COF-300 will not only allow fast gas

permeation, but also lead to efficient gas discrimination based on size differences of these light gases.[32] To further probe the gas affinity of COF-300, different gas sorption isotherms (CO_2, CH_4, and N_2) were collected for COF-300 crystals at 273 K (Fig. S3†) and 298 K up to 1 bar (Fig. 1g). At 298 K and 1 bar, COF-300 exhibits a CO_2 uptake of 23.5 $cm^3\ g^{-1}$, which is 94% and 571% higher than that of CH_4 (12.1 $cm^3\ g^{-1}$) and N_2 (3.5 $cm^3\ g^{-1}$), respectively. The different gas affinity of COF-300 could be rationalized by the variances in gas polarizabilities (*e.g.*, CO_2: 26.3 $\times$ 10^{-25} cm^3, CH_4: 26.0 $\times$ 10^{-25} cm^3, and N_2: 17.6 $\times$ 10^{-25} cm^3).[32] For gas molecules with higher polarizability, they tend to be more easily polarized by the pore walls and adsorbed more strongly within the framework. To quantitatively characterize these interactions between COF-300 and gases, the isosteric heats of adsorption (Q_{st}) with acceptable accuracy for CO_2, CH_4 and N_2 were calculated on the basis of temperature-dependent isotherms collected at 273 and 298 K using the Clausius–Clapeyron equation.[33] It is worth noting that uncertainties may still arise during the calculation because of only two isotherms used here. As shown in Fig. S4a,† the low-coverage Q_{st} value of CO_2 (17.7 kJ mol^{-1}) is higher than that of CH_4 (15.0 kJ mol^{-1}) and N_2 (9.8 kJ mol^{-1}), validating that COF-300 exhibits the strongest interaction with CO_2 among the three target gases. Furthermore, the CO_2/CH_4 and CO_2/N_2 selectivities of COF-300 were calculated from single gas sorption isotherms based on the ideal adsorption solution theory (IAST, Fig. S4b†).[23] For equal molar gas mixtures at 298 K and 1 bar, COF-300 demonstrates IAST selectivities of 1.8 and 9.9 for CO_2/CH_4 and CO_2/N_2, respectively, indicating that COF-300 is favorable for enhancing the CO_2/N_2 solubility selectivity inside the resultant MMMs.

Characterization of COF-300 based MMMs

To explore the generality of COF-300 in advancing the separation performance of pure polymeric membranes, a glassy polymer (6FDA-DAM) and a rubbery polymer (Pebax) were adopted as the polymer matrixes to fabricate MMMs. It is widely accepted that there exists an optimum filler content in MMMs, beyond which the appearance of filler agglomeration will induce the formation of nonselective voids that lead to the fast loss of membrane gas selectivity.[34] Therefore, MMMs with various COF-300 filler contents (2, 5, 7, 10 and 15 wt%) were fabricated both in 6FDA-DAM and Pebax systems to explore the optimum filler content for COF-300. The filler dispersion status and polymer-filler interfacial morphologies in all MMMs were characterized by FESEM (Fig. 2a–f, S5 and S6†). Both pure 6FDA-DAM and Pebax membranes exhibit dense and defect-free microstructures, in good agreement with the typical morphology of pure polymeric membranes.[35] The homogeneous distribution of COF-300 crystals in the 6FDA-DAM matrix can be clearly observed when the filler content ranges from 2–7 wt%. The existence of polymer veins suggests a favorable interaction between the polymer matrix and the COF fillers. Nevertheless, as the filler content approaches 10 wt%, COF-300 tends to agglomerate and fails to be efficiently wrapped by polymer chains. This becomes even worse when the filler content reaches 15 wt%, as reflected by the serious filler agglomeration disrupting the continuous polymer chain packing in the corresponding MMM. As for the rubbery Pebax system, the soft polyether segments in Pebax backbones can efficiently wrap COF-300 fillers, leading to an optimum filler content of 10 wt%, which is slightly higher than that of the glassy 6FDA-DAM system (7 wt%). This suggests an effective

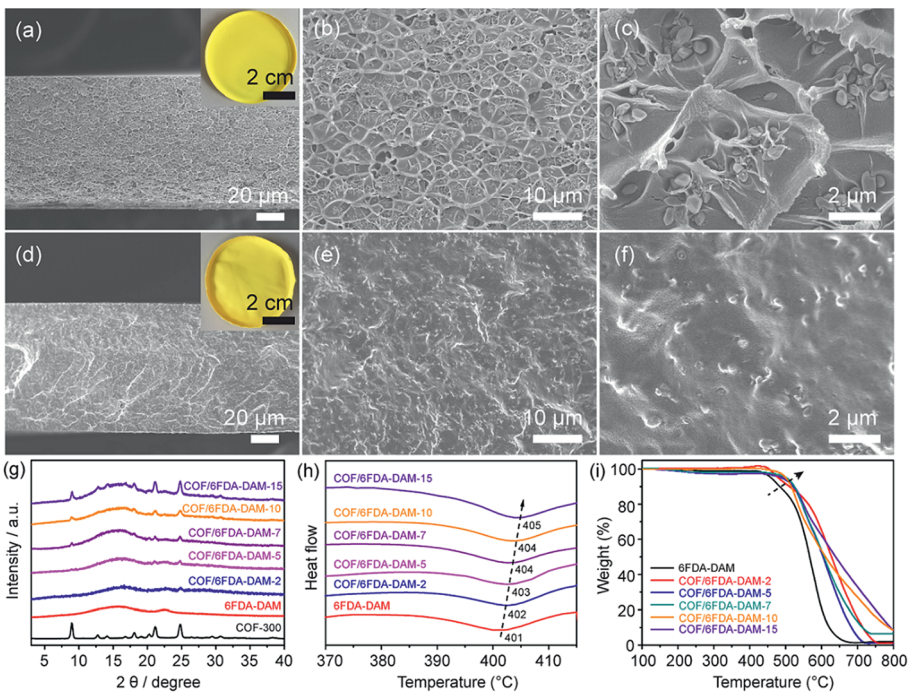

Fig. 2 Membrane cross-sectional FESEM images of (a)–(c): the COF-300/6FDA-DAM-7 MMM and (d)–(f) COF-300/Pebax-10 MMM. (g) PXRD patterns of COF-300 fillers and COF-300/6FDA-DAM series MMMs. (h) DSC and (i) TGA curves of COF-300/6FDA-DAM series MMMs.

strategy to further enhance the optimum filler contents in MMMs by increasing the percentage of rubbery segments in a copolymer matrix.

The mixing properties of all membranes were recorded by FTIR spectra. As shown in Fig. S7,† in the COF-300/6FDA-DAM system, the characteristic peaks assigned to the 6FDA-DAM polymer are well maintained in all MMMs without any noticeable peak shifts or intensity changes, indicating that COF-300 fillers are physically wrapped by 6FDA-DAM chains without strong chemical interactions. As for the COF-300/Pebax system, the characteristic peaks ascribing to the Pebax matrix can nearly all be observed in the corresponding MMMs, except for the N–H stretching at 3263 cm^{-1}, which experiences an intensity decrease and eventually disappears with the incorporation of COF-300 fillers (Fig. S8†). This could be rationalized by the hydrogen bonding between the N–H groups in Pebax and the C=N groups in COF-300 fillers.[30] The X-ray diffraction (XRD) patterns of all membranes were recorded to evaluate the crystallinity of COF-300 fillers inside the polymer matrixes. As shown in Fig. 2g, pure 6FDA-DAM shows a major broad peak at $2\theta = 15.9°$ and a minor broad peak at $2\theta = 22.6°$, confirming its amorphous nature. As for the COF-300/6FDA-DAM MMMs, the characteristic diffraction peaks ascribing to 3D COF fillers become more prominent as the filler content increases in the membranes, implying that COF-300 maintains its good crystallinity during the membrane fabrication process. Similar results were found in Pebax series membranes, demonstrating obvious characteristic peaks originating from COF-300 fillers especially when the filler content reaches 10 wt% (Fig. S9†). Notably, this strongly verifies the good chemical stability of imine-based COF-300 as it can survive in the water/ethanol mixture adopted to prepare the membrane casting suspension.

The specific polymer-filler interfacial interactions can be revealed by the changes in the glass transition temperature (T_g) of the membranes. An increase in the membrane T_g can be ascribed to the reduced polymer chain mobility and polymer rigidification at the outer surface of the fillers, indicating favorable polymer-filler interactions. More importantly, these rigidified polymer chains are capable of achieving better size-discriminative separation, leading to higher membrane selectivity at the cost of gas permeability.[18] As shown in Fig. 2h, the T_g of the pure 6FDA-DAM membrane is 401 °C, which gradually shifts to higher values with the addition of COF-300 fillers, and eventually reaches 405 °C for the MMM containing 15 wt% of COF-300 fillers. As for the Pebax system, the pure Pebax membrane demonstrates a T_g of −46 °C originating from the soft polyether segments, and the membrane T_g increases to −34 °C for the MMM with 15 wt% of COF-300 filler loading (Fig. S10†). The similar organic nature of the polymer matrix and COF fillers sets the foundation of their favorable interactions. Moreover, the effective hydrogen bonding between the Pebax matrix and COF-300 fillers further promotes their interfacial interactions, as reflected by a larger T_g increase in the Pebax system (12 °C) compared to that in the 6FDA-DAM system (4 °C). The polymer-filler interactions can also be proved by the membrane thermal stability determined by TGA. As shown in Fig. 2i, the pure 6FDA-DAM membrane is thermally stable up to 430 °C, after which it experiences a fast weight loss owing to the degradation of its backbones in the air. With the incorporation of COF-300 fillers, the thermal stability of the resultant MMMs gradually increases. For instance, the MMM with 15 wt% COF-300 fillers exhibits a decomposition temperature of 490 °C, confirming the enhanced membrane thermal stability induced by COF fillers. A similar trend was observed in the Pebax system (Fig. S11†). For example, the temperature for 10 wt% membrane weight loss is 340 °C for the pure Pebax membrane and 382 °C for the COF-300/Pebax-15 MMM, also indicating strong polymer-filler interactions in MMMs.

The mechanical properties of all the membranes were analysed by tensile tests. As shown in Fig. S12 and Table S1,† both 6FDA-DAM and Pebax systems demonstrate enhanced Young's moduli with the gradual increase of COF-300 filler contents in the MMMs. Specifically, the membrane's Young's modulus exhibits an 18.5% increase from 1.62 GPa of the pure 6FDA-DAM membrane to 1.92 GPa of the COF-300/6FDA-DAM-7 MMM. The enhancement in the membrane's Young's modulus is even more pronounced in the Pebax system, which demonstrates a 104.1% increase from 3.42 MPa of the pure Pebax membrane to 6.98 MPa of the COF-300/Pebax-10 MMM, confirming stronger interfacial interactions in the Pebax system. Nevertheless, in both systems, the membrane's Young's modulus experiences a fast loss at high filler contents due to the appearance of filler agglomeration, which seriously deteriorates the membrane's mechanical strength. Moreover, compared with pure polymeric membranes, the maximum tensile strength and the elongation at break monotonically decreases with the addition of COF-300, which could be rationalized by the reduced membrane ductility induced by polymer chain rigidification at the polymer-filler interfaces.[36]

Gas separation performance of COF-300-based MMMs

The gas separation performance of all membranes was evaluated with the feed of an equal molar mixture of CO_2/CH_4 or CO_2/N_2 at 25 °C with a transmembrane pressure of 1 bar. Each type of membrane was replicated at least three times to ensure the good reproducibility and reliability of the results. As shown in Fig. 3, with the incorporation of suitable amounts of COF-300 fillers, both 6FDA-DAM and Pebax systems demonstrate a concurrent increase in gas permeability and selectivity. The increase in gas permeability can be attributed to the highly porous nature of 3D COF fillers, providing fast gas transport paths inside the resultant membranes. Despite that polymer chain rigidification may partially reduce the membrane gas permeability, the final MMMs with the optimum filler content still exhibit a substantially enhanced CO_2 permeability, as demonstrated by a ~52% and ~57% increase in CO_2 permeability in the 6FDA-DAM and Pebax systems, respectively. Meanwhile, the ultrasmall 4 Å pores in COF-300 can discriminate gas molecules based on their size differences so as to achieve selective permeation of smaller gas molecules (*e.g.*, CO_2) over larger ones (*e.g.*, CH_4 or N_2), leading to the increase in membrane CO_2/CH_4 and CO_2/N_2 selectivities. Such phenomena

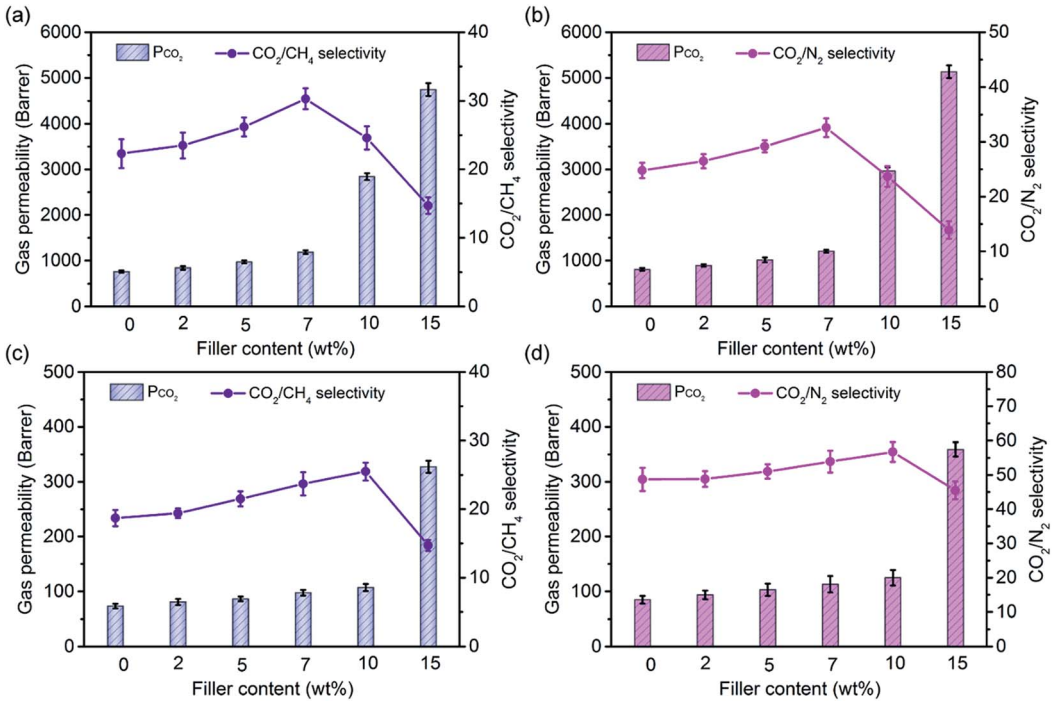

Fig. 3 The effect of the COF-300 filler content on membrane separation performance tested at 25 °C with a transmembrane pressure of 1 bar. (a) CO_2/CH_4 and (b) CO_2/N_2 separation performance of COF-300/6FDA-DAM series MMMs. (c) CO_2/CH_4 and (d) CO_2/N_2 separation performance of COF-300/Pebax series MMMs.

have been well-documented in other porous materials with ultrasmall pores, such as ZIF-8 (3.4 Å),[37] SNW-1 (5 Å)[32] and CuBDC (5.4 Å).[38] In contrast, for MMMs containing 2D COF fillers with relatively large pores (>8 Å), a slight increase or even decrease in gas pair selectivity has been frequently observed owing to the lack of size-selective pores in these fillers (Table S2†). This strongly validates that 3D COF fillers with ultrasmall pores are promising candidates in MMMs for enhancing the membrane gas discrimination ability. Notably, all MMMs exhibit a monotonically increased selectivity for both CO_2/CH_4 and CO_2/N_2 mixtures with the addition of COF-300 fillers before the appearance of filler agglomeration, further corroborating their defect-free microstructures because of the good compatibility between the polymer matrix and the organic fillers. Nevertheless, the sharp selectivity drop and fast permeability increase in COF-300/6FDA-DAM-10 and COF-300/Pebax-15 MMMs unambiguously suggest the existence of nonselective voids inside these membranes owing to filler agglomeration, matching well with the membrane FESEM and mechanical strength results.

Prediction of intrinsic gas separation performance of COF-300

The intrinsic gas separation performance of COF-300 can be predicted from the experimental membrane separation data based on the Maxwell model, which was originally developed for the estimation of dielectric properties of hybrid materials.[39] This model has now been widely adopted to predict the separation performance of MMMs at low filler contents, and it can be written as follows:

$$P_{\text{eff}} = P_{\text{c}}\left[\frac{P_{\text{d}} + 2P_{\text{c}} - 2\varnothing_{\text{d}}(P_{\text{c}} - P_{\text{d}})}{P_{\text{d}} + 2P_{\text{c}} + \varnothing_{\text{d}}(P_{\text{c}} - P_{\text{d}})}\right] \quad (3)$$

where P_{eff} refers to the effective gas permeability of MMMs, P_{c} and P_{d} refer to the gas permeability of the continuous polymer matrix phase and the dispersed filler phase, respectively, $\varnothing_{\text{d}}$ refers to the volume percentage of the dispersed filler phase in the MMMs. Fillers were incorporated into the membranes based on the weight percentage, which should be converted into volume percentage for the Maxwell prediction. The crystal density of COF-300 is 0.66 g cm^{-3},[28] and the densities of 6FDA-DAM and Pebax are assumed to be 1.33 and 1.14 g cm^{-3}, respectively.[40,41] Given the good interfacial compatibility between the polymer matrix and COF-300 fillers in both systems at a low filler content (*e.g.*, 2 wt%), it is reasonable to back calculate the intrinsic gas separation performance of COF-300 through the Maxwell model, which further allows the prediction of gas separation performance of all MMMs with other filler contents (*e.g.*, 5, 7, 10 and 15 wt%). Moreover, these predicted gas separation performances of MMMs could be compared with the experimental results to further probe the separation mechanism of these MMMs. Detailed results are listed in Tables S3, and S4† and shown in Fig. 4. Interestingly, the intrinsic separation performance of COF-300 was found to vary in different polymer systems. For instance, for CO_2/CH_4 separation, COF-300 was estimated to demonstrate a CO_2 permeability of 9830 barrer and a CO_2/CH_4 selectivity of 75 in the 6FDA-DAM system, while it exhibits a CO_2 permeability of 8850 barrer and a CO_2/CH_4 selectivity of 110 in the Pebax system. These variances can be understood considering that polymer

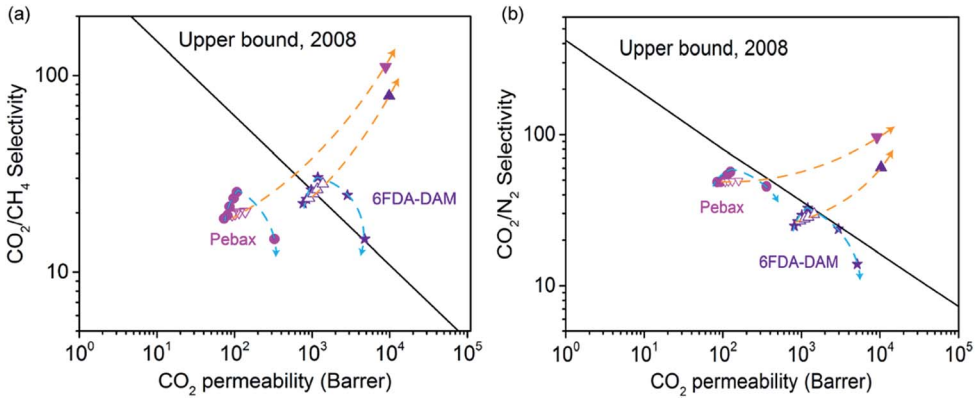

Fig. 4 Robeson upper bound plots for (a) CO_2/CH_4 and (b) CO_2/N_2 of both 6FDA-DAM and Pebax systems. The solid spheres and stars represent experimental values, while empty triangles represent predicted values for both systems based on the Maxwell model. Solid triangles represent the predicted separation performance of the pure COF-300 membrane, showing its excellent intrinsic separation performance on the upper bound plots. Yellow and blue curves represent predicted and experimental separation performance of MMMs, respectively.

rigidification in the two polymer systems will inevitably lead to calculation deviations. Besides, the rubbery polyether segments and hydrogen bonding between the Pebax matrix and COF-300 fillers synergistically enhance polymer-filler interactions in the Pebax system, leading to even stronger polymer chain rigidification that increases membrane selectivity at the cost of gas permeability. This trend can be clearly observed in Fig. 4, where the experimental CO_2/CH_4 and CO_2/N_2 selectivities of the Pebax system are much higher than those values predicted from the Maxwell model. As for the 6FDA-DAM system, the experimental data are close to the predicted data before the filler agglomeration, indicating a good match between the two phases in this system. Most importantly, regardless of the glassy or rubbery system, the estimated intrinsic gas separation performance of COF-300 far exceeds that of the 2008 Robeson upper bound limits, highlighting the great potential of fabricating pure polycrystalline COF-300 membranes for efficient CCS in the future.

Effect of the transmembrane pressure

Considering that industrial gas separation processes are often conducted at relatively high pressures (*e.g.*, up to 60 bar for natural gas sweetening),[3] it is therefore necessary to investigate the influence of transmembrane pressures on the separation performance of the as-prepared membranes. The COF-300/6FDA-DAM-7 and COF-300/Pebax-10 MMMs were explored here owing to their optimum separation performance in each system. Meanwhile, the separation performance of pure 6FDA-DAM and Pebax membranes at varying pressures was recorded as comparison. As shown in Fig. 5a and b and S13,† both pure 6FDA-DAM and Pebax membranes experience a simultaneous decrease in CO_2 permeability and CO_2/CH_4, CO_2/N_2 selectivities when the transmembrane pressure increases from 1 bar to 8 bar, corresponding well to the trend observed in the literature.[42,43] Nevertheless, the decrease of CO_2 permeability in the pure 6FDA-DAM membrane is ~21%, which is slightly higher than that of the ~15% decrease in the pure Pebax membrane. For the glassy 6FDA-DAM system, this decrease at high pressures mainly originates from the saturation of Langmuir sorption sites based on the dual sorption model.[23] As for the rubbery Pebax system, the decrease of CO_2 permeability could be ascribed to the reduced membrane free volume caused by the compaction of rubbery polymer chains under higher pressures.[44] With the incorporation of porous COF-300 fillers, more Langmuir sorption sites are introduced into the membrane systems. In addition, rigidified polymer chains at the polymer-filler interfaces render both systems more resistant to compaction effects at high pressures. Therefore, the decreasing trend of CO_2 permeability is efficiently reduced in MMMs, as reflected by the ~16% decrease in the 6FDA-DAM-based MMM and the ~9% decrease in the Pebax-based MMM. Moreover, the CO_2/CH_4 and CO_2/N_2 selectivities of both MMMs are still much higher than those of the corresponding pure membranes at higher pressures (*e.g.*, 8 bar), highlighting the great potential of as-prepared MMMs for CCS under more realistic conditions.

Long term stability of COF-300-based MMMs

The long term stability of membranes plays a crucial role in realizing the full potential of membrane technology for industrial applications. The as-prepared COF-300/6FDA-DAM-7 and COF-300/Pebax-10 MMMs were evaluated for a 100 h continuous separation of a CO_2/CH_4 mixture at 25 °C and a transmembrane pressure of 4 bar. As shown in Fig. 5c and d, both MMMs demonstrate a rather stable performance during the initial 40 h, indicating their good operational stability that is desired for industrial use. Subsequently, moisture (relative humidity: ~85%) was introduced into both systems considering that a trace amount of water may severely influence the membrane separation performance.[45] Interestingly, these two polymer systems react differently toward moisture. As for the glassy 6FDA-DAM system, the gas permeability of the membrane decreases while the CO_2/CH_4 selectivity increases with the introduction of moisture. The reduction of gas permeability could be attributed to the occupation of the membrane free volume by water molecules trapped inside the

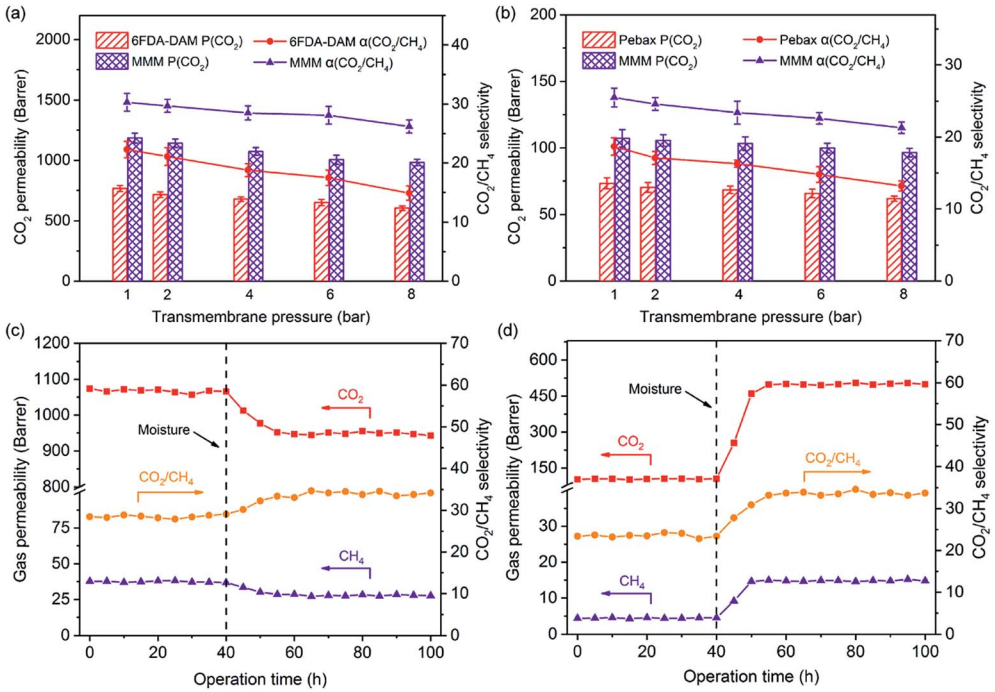

Fig. 5 Transmembrane pressure influence on the membrane CO_2/CH_4 separation performance of (a) 6FDA-DAM and (b) Pebax systems tested at 25 °C. Long-term stability for CO_2/CH_4 separation of MMMs in (c) 6FDA-DAM and (d) Pebax systems tested at 25 °C with a transmembrane pressure of 4 bar.

membrane.[46] These water molecules are beneficial for the solubility increase of CO_2 in the membrane, compensating its diffusivity loss due to the reduction of the membrane free volume.[30] Therefore, the CO_2 permeability loss (~12%) is smaller than that of CH_4 (~27%), leading to the ~23% increase of membrane CO_2/CH_4 selectivity. As for the Pebax system, the membrane gas permeability quickly increases accompanied by an enhancement in CO_2/CH_4 selectivity with the introduction of moisture. The increase in gas permeability is understandable considering the swelling of the soft polyether segments caused by water molecules. Moreover, the hydrophilic Pebax matrix can retain a high water uptake that largely enhances the membrane CO_2 solubility, further promoting CO_2 permeation through the membrane.[18] The CO_2 permeability increase is ~380%, much higher than the ~220% increase of CH_4 permeability, resulting in the ~42% enhancement of membrane selectivity. Notably, both MMMs can maintain their impressive separation performance after being stabilized in the presence of moisture, highlighting the good chemical stability of both polymer matrixes and COF-300 fillers.

Functionalization of COF-300 with PEI

The interfacial design in MMMs achieved by grafting porous fillers with other functional groups has been demonstrated to be a powerful strategy in enhancing the membrane separation performance. Up till now, numerous porous fillers, including MCM-41,[18] ZIF-8,[47] MIL-101(Cr),[48] and UiO-66-NH_2,[49] have been functionalized with diversified polymers to enable the fabrication of high-performance MMMs. However, as far as we know, this strategy has not been applied to COF fillers yet. Consequently, PEI was adopted here to functionalize COF-300 fillers (denoted as COF@PEI) to further explore their potential in MMMs (Fig. 6a). The terminal –CHO and –NH_2 groups at the surface of COF-300 can allow either covalent linkages or hydrogen bonding between COF-300 and PEI chains in the composite material, respectively. Moreover, the abundant amine groups in PEI can not only improve the polymer-filler affinity by forming hydrogen bonds at the interfaces, but also facilitate the sorption of CO_2 over CH_4 and N_2 in the membrane. As shown in Fig. S14,† the FTIR spectrum of COF@PEI demonstrates two prominent peaks at 2820 cm^{-1} and 1045 cm^{-1} originating from the N–H and C–N stretching vibrations of PEI, respectively. Moreover, the characteristic C=N vibration at 1620 cm^{-1} of COF-300 remains unchanged in COF@PEI, suggesting that the PEI functionalization did not alter the structural integrity of the original COF-300. COF@PEI exhibits nearly identical PXRD patterns compared to COF-300, indicating the maintenance of good COF crystallinity in the composite material (Fig. S15†). The diffraction peaks in COF@PEI are slightly broadened owing to the formation of PEI coatings on COF-300, which is further evidenced by the smooth surface of COF@PEI particles observed under FESEM and TEM (Fig. 6b and c). The specific content of PEI coating in the hybrid was estimated to be 17 wt% based on TGA (Fig. S16†). The BET surface area of COF@PEI is 1020 $m^2\ g^{-1}$ (Fig. S17†), 15.6% smaller than that of the original COF-300 due to the incorporation of nonporous PEI chains. On the other hand, the detectable BET surface area of COF@PEI confirms that the pores of COF-300 are not fully blocked by the PEI coating. As

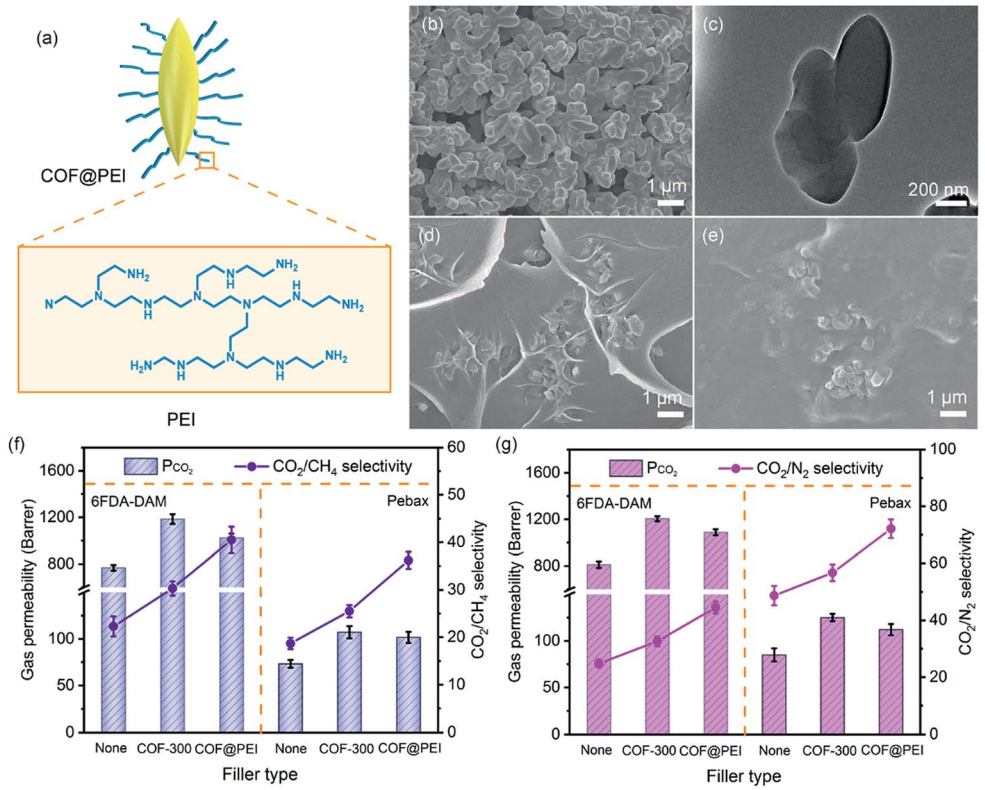

Fig. 6 (a) Illustration of the PEI grafting on the surface of COF-300 in COF@PEI. (b) FESEM and (c) TEM images of COF@PEI particles. Membrane cross-sectional FESEM images of (d) COF@PEI/6FDA-DAM-7 and (e) COF@PEI/Pebax-10 MMMs. (f) CO_2/CH_4 and (g) CO_2/N_2 separation performance of pure polymeric membranes and MMMs containing different fillers.

shown in Fig. S18,† COF@PEI demonstrates an impressive CO_2 uptake of 48.9 $cm^3\ g^{-1}$ at 273 K and a low-uptake CO_2 Q_{st} of 21.8 kJ mol^{-1}, much higher than those of COF-300 under identical conditions (CO_2 uptake: 31.4 $cm^3\ g^{-1}$, CO_2 Q_{st}: 17.7 kJ mol^{-1}). Besides, the CO_2/N_2 and CO_2/CH_4 IAST selectivities of COF@PEI are 17.6 and 3.7, respectively, also much larger than those of bare COF-300 (CO_2/N_2: 9.9, CO_2/CH_4: 1.8). These gas sorption results unambiguously confirm that the functionalization of COF-300 with amine-rich PEI can greatly enhance the CO_2-philicity of the hybrid material, which should eventually benefit the selective sorption of CO_2 over CH_4 and N_2 inside MMMs.

Given that the optimum COF-300 filler content in the 6FDA-DAM and Pebax matrixes are 7 and 10 wt%, respectively, COF@PEI fillers were also added into each system based on the corresponding optimum content. As shown in Fig. 6d, e and S19,† COF@PEI fillers are strongly wrapped by the polymer chains regardless of the polymer type, leading to defect-free microstructures in both systems. This could be attributed to the similar organic nature of the two phases and the strong hydrogen bonding between the abundant $-NH_2$ groups in PEI and C=O groups in both polymers.[48] Moreover, extra hydrogen bonding formed at the N–H and C–O sites in Pebax could be possible, further promoting the polymer-filler interfacial compatibility. The CO_2/CH_4 and CO_2/N_2 separation performance of COF@PEI-based MMMs was tested at 25 °C with a transmembrane pressure of 1 bar, and is compared with those of pure polymeric membranes and COF-300-based MMMs in Fig. 6f and g. Interestingly, among these three types of membranes, COF@PEI-based MMMs demonstrate the highest gas pair selectivity while COF-300-based MMMs demonstrate the highest CO_2 permeability. For example, in the 6FDA-DAM system for CO_2/CH_4 separation, the COF@PEI-based MMM exhibits a CO_2/CH_4 selectivity of 40.5, which is 33.7% and 81.6% higher than that of the COF-300-based MMM and pure 6FDA-DAM membrane, respectively. However, the CO_2 permeability of the COF@PEI-based MMM is 1023 barrer, which is 13.7% lower than that of the COF-300-based MMM while 33.4% higher than that of the pure membrane. Furthermore, MMMs containing other COF@PEI contents (10–20 wt% for 6FDA-DAM; 15–25 wt% for Pebax) have been fabricated and tested for CO_2/CH_4, CO_2/N_2 separations. As shown in Fig. S20, Tables S5 and S6,† with the addition of COF@PEI fillers (7–10 wt% for 6FDA-DAM; 10–20 wt% for Pebax), an increased CO_2 permeability accompanied by a decreased CH_4 or N_2 permeability has been observed in the resultant MMMs, leading to an increased gas pair selectivity. This could be attributed to the severe polymer chain rigidification caused by the strong polymer-filler interactions because of the PEI coating. This corresponds well to the previous reports on other porous fillers, including UiO-66-NH_2,[50] ZIF-7-NH_2 (ref. 51) and PEI-MCM-41.[18] The optimum filler contents for COF@PEI reach 10 wt% and 20 wt% for the 6FDA-DAM and Pebax systems, respectively, which are higher than those of pure COF-300 in the corresponding system (7 wt%

for 6FDA-DAM and 10 wt% for Pebax), further confirming the effectiveness of PEI coating in enhancing polymer-filler interfacial compatibility. Finally, COF@PEI-based MMMs exhibit a largely enhanced CO_2/CH_4 and CO_2/N_2 separation performance that is close to or even above the Robeson upper bound (Fig. S21†). These results strongly validate that COF@PEI fillers are promising candidates for the preparation of high-performance MMMs for industrial CCS applications.

Conclusions

In summary, we incorporated a 3D COF, COF-300, into two different polymer matrixes, including glassy 6FDA-DAM and rubbery Pebax, to explore the potential of 3D COF fillers in MMMs. Defect-free MMMs were successfully prepared at relatively low COF-300 filler contents, demonstrating the good polymer-filler interfacial compatibility owing to the similar organic nature of these two phases. Besides, the well-defined pores of COF-300 fillers can construct fast gas permeation channels to increase the membrane gas permeability, while the rigidified polymer chains on the filler surface and the ultrasmall pores of COF-300 can lead to increased gas pair selectivity, largely advancing the separation performance of pure polymeric membranes toward or even above the 2008 Robeson upper bounds. Moreover, COF-300-based MMMs exhibit good anti-pressure and anti-moisture performance, accompanied by a decent long term stability originating from the excellent chemical stability of both polymer matrixes and COF-300 fillers. Finally, pure COF-300 could be further functionalized with PEI coating, leading to the formation of COF@PEI fillers that demonstrate enhanced polymer-filler affinity. This offers a promising strategy toward the design and fabrication of high performance MMMs for CCS. We envision that this work will shed light on the exploration of more novel COF fillers, including ionic COFs, heteropore COFs, *etc.*, in MMMs for industrial separations.

Conflicts of interest

There are no conflicts to declare.

Acknowledgements

This work is supported by the National University of Singapore (CENGas R-261-508-001-646), the Ministry of Education - Singapore (MOE AcRF Tier 1 R-279-000-472-112, R-279-000-540-114), and the Agency for Science, Technology and Research (PSF 1521200078, IRG A1783c0015, IAF-PP A1789a0024).

Notes and references

1 M. Oschatz and M. Antonietti, *Energy Environ. Sci.*, 2018, **11**, 57–70.
2 R. S. Haszeldine, *Science*, 2009, **325**, 1647–1652.
3 R. W. Baker and K. Lokhandwala, *Ind. Eng. Chem. Res.*, 2008, **47**, 2109–2121.
4 W. J. Koros and C. Zhang, *Nat. Mater.*, 2017, **16**, 289–297.
5 N. B. McKeown and P. M. Budd, *Chem. Soc. Rev.*, 2006, **35**, 675–683.
6 S. Qiu, M. Xue and G. Zhu, *Chem. Soc. Rev.*, 2014, **43**, 6116–6140.
7 S. Hanioka, T. Maruyama, T. Sotani, M. Teramoto, H. Matsuyama, K. Nakashima, M. Hanaki, F. Kubota and M. Goto, *J. Membr. Sci.*, 2008, **314**, 1–4.
8 X. Wang, C. Chi, K. Zhang, Y. Qian, K. M. Gupta, Z. Kang, J. Jiang and D. Zhao, *Nat. Commun.*, 2017, **8**, 14460.
9 L. M. Robeson, *J. Membr. Sci.*, 2008, **320**, 390–400.
10 W. F. Yong, Z. K. Lee, T. S. Chung, M. Weber, C. Staudt and C. Maletzko, *ChemSusChem*, 2016, **9**, 1953–1962.
11 F. Y. Li, Y. Xiao, T. S. Chung and S. Kawi, *Macromolecules*, 2012, **45**, 1427–1437.
12 I. Rose, C. G. Bezzu, M. Carta, B. Comesana-Gandara, E. Lasseuguette, M. C. Ferrari, P. Bernardo, G. Clarizia, A. Fuoco, J. C. Jansen, K. E. Hart, T. P. Liyana-Arachchi, C. M. Colina and N. B. McKeown, *Nat. Mater.*, 2017, **16**, 932.
13 Y. Cheng, Y. Ying, S. Japip, S.-D. Jiang, T.-S. Chung, S. Zhang and D. Zhao, *Adv. Mater.*, 2018, **30**, 1802401.
14 Y. Cheng, Z. Wang and D. Zhao, *Ind. Eng. Chem. Res.*, 2018, **57**, 4139–4169.
15 J. Dechnik, J. Gascon, C. J. Doonan, C. Janiak and C. J. Sumby, *Angew. Chem., Int. Ed.*, 2017, **56**, 9292–9310.
16 Y. Li, T. S. Chung, C. Cao and S. Kulprathipanja, *J. Membr. Sci.*, 2005, **260**, 45–55.
17 S. Matteucci, V. A. Kusuma, D. Sanders, S. Swinnea and B. D. Freeman, *J. Membr. Sci.*, 2008, **307**, 196–217.
18 H. Wu, X. Li, Y. Li, S. Wang, R. Guo, Z. Jiang, C. Wu, Q. Xin and X. Lu, *J. Membr. Sci.*, 2014, **465**, 78–90.
19 X. Zhu, C. Tian, C.-L. Do-Thanh and S. Dai, *ChemSusChem*, 2017, **10**, 3304–3316.
20 G. Liu, V. Chernikova, Y. Liu, K. Zhang, Y. Belmabkhout, O. Shekhah, C. Zhang, S. Yi, M. Eddaoudi and W. J. Koros, *Nat. Mater.*, 2018, **17**, 283–289.
21 Y. Cheng, X. Wang, C. Jia, Y. Wang, L. Zhai, Q. Wang and D. Zhao, *J. Membr. Sci.*, 2017, **539**, 213–223.
22 Y. Cheng, S. R. Tavares, C. M. Doherty, Y. Ying, E. Sarnello, G. Maurin, M. R. Hill, T. Li and D. Zhao, *ACS Appl. Mater. Interfaces*, 2018, **10**, 43095–43103.
23 Z. Kang, Y. Peng, Y. Qian, D. Yuan, M. A. Addicoat, T. Heine, Z. Hu, L. Tee, Z. Guo and D. Zhao, *Chem. Mater.*, 2016, **28**, 1277–1285.
24 M. Shan, B. Seoane, E. Rozhko, A. Dikhtiarenko, G. Clet, F. Kapteijn and J. Gascon, *Chem.–Eur. J.*, 2016, **22**, 14467–14470.
25 B. P. Biswal, H. D. Chaudhari, R. Banerjee and U. K. Kharul, *Chem.–Eur. J.*, 2016, **22**, 4695–4699.
26 H. M. El-Kaderi, J. R. Hunt, J. L. Mendoza-Cortés, A. P. Côté, R. E. Taylor, M. O'Keeffe and O. M. Yaghi, *Science*, 2007, **316**, 268–272.
27 T. Ma, J. Li, J. Niu, L. Zhang, A. S. Etman, C. Lin, D. Shi, P. Chen, L.-H. Li, X. Du, J. Sun and W. Wang, *J. Am. Chem. Soc.*, 2018, **140**, 6763–6766.
28 F. J. Uribe-Romo, J. R. Hunt, H. Furukawa, C. Klöck, M. O'Keeffe and O. M. Yaghi, *J. Am. Chem. Soc.*, 2009, **131**, 4570–4571.

29 S. Kandambeth, A. Mallick, B. Lukose, M. V. Mane, T. Heine and R. Banerjee, *J. Am. Chem. Soc.*, 2012, **134**, 19524–19527.
30 X. Li, Z. Jiang, Y. Wu, H. Zhang, Y. Cheng, R. Guo and H. Wu, *J. Membr. Sci.*, 2015, **495**, 72–80.
31 J. L. Segura, M. J. Mancheno and F. Zamora, *Chem. Soc. Rev.*, 2016, **45**, 5635–5671.
32 X. Gao, X. Zou, H. Ma, S. Meng and G. Zhu, *Adv. Mater.*, 2014, **26**, 3644–3648.
33 J. Dong, Y. Wang, G. Liu, Y. Cheng and D. Zhao, *CrystEngComm*, 2017, **19**, 4899–4904.
34 X. Wu, Z. Tian, S. Wang, D. Peng, L. Yang, Y. Wu, Q. Xin, H. Wu and Z. Jiang, *J. Membr. Sci.*, 2017, **528**, 273–283.
35 Q. Song, S. Cao, P. Zavala-Rivera, L. Ping Lu, W. Li, Y. Ji, S. A. Al-Muhtaseb, A. K. Cheetham and E. Sivaniah, *Nat. Commun.*, 2013, **4**, 1918.
36 X. Wu, W. Liu, H. Wu, X. Zong, L. Yang, Y. Wu, Y. Ren, C. Shi, S. Wang and Z. Jiang, *J. Membr. Sci.*, 2018, **548**, 309–318.
37 X. Zhang, T. Zhang, Y. Wang, J. Li, C. Liu, N. Li and J. Liao, *J. Membr. Sci.*, 2018, **560**, 38–46.
38 T. Rodenas, I. Luz, G. Prieto, B. Seoane, H. Miro, A. Corma, F. Kapteijn, F. X. Llabrés i Xamena and J. Gascon, *Nat. Mater.*, 2015, **14**, 48–55.
39 T. S. Chung, L. Y. Jiang, Y. Li and S. Kulprathipanja, *Prog. Polym. Sci.*, 2007, **32**, 483–507.
40 W. Xu, D. R. Paul and W. J. Koros, *J. Membr. Sci.*, 2003, **219**, 89–102.
41 A. Car, C. Stropnik, W. Yave and K.-V. Peinemann, *J. Membr. Sci.*, 2008, **307**, 88–95.
42 V. Nafisi and M.-B. Hägg, *Sep. Purif. Technol.*, 2014, **128**, 31–38.
43 X. Li, Y. Cheng, H. Zhang, S. Wang, Z. Jiang, R. Guo and H. Wu, *ACS Appl. Mater. Interfaces*, 2015, **7**, 5528–5537.
44 P. D. Sutrisna, J. Hou, H. Li, Y. Zhang and V. Chen, *J. Membr. Sci.*, 2017, **524**, 266–279.
45 R. W. Baker and B. T. Low, *Macromolecules*, 2014, **47**, 6999–7013.
46 C. Tsvigu, E. Pavesi, M. G. De Angelis and M. Giacinti Baschetti, *J. Membr. Sci.*, 2015, **485**, 60–68.
47 Z. Wang, D. Wang, S. Zhang, L. Hu and J. Jin, *Adv. Mater.*, 2016, **28**, 3399–3405.
48 Q. Xin, J. Ouyang, T. Liu, Z. Li, Z. Li, Y. Liu, S. Wang, H. Wu, Z. Jiang and X. Cao, *ACS Appl. Mater. Interfaces*, 2015, **7**, 1065–1077.
49 K. Xie, Q. Fu, J. Kim, H. Lu, Y. He, Q. Zhao, J. Scofield, P. A. Webley and G. G. Qiao, *J. Membr. Sci.*, 2017, **535**, 350–356.
50 B. Ghalei, K. Sakurai, Y. Kinoshita, K. Wakimoto, A. P. Isfahani, Q. Song, K. Doitomi, S. Furukawa, H. Hirao, H. Kusuda, S. Kitagawa and E. Sivaniah, *Nat. Energy*, 2017, **2**, 17086.
51 L. Xiang, L. Sheng, C. Wang, L. Zhang, Y. Pan and Y. Li, *Adv. Mater.*, 2017, **29**, 1606999–1607006.